

Meaningful Scales Detection along Digital Contours for Unsupervised Local Noise Estimation

Bertrand Kerautret and Jacques-Olivier Lachaud

Abstract—The automatic detection of noisy or damaged parts along digital contours is a difficult problem since it is hard to distinguish between information and perturbation without further a priori hypotheses. However, solving this issue has a great impact on numerous applications, including image segmentation, geometric estimators, contour reconstruction, shape matching, or image edition. We propose an original strategy to detect what the relevant scales are at which each point of the digital contours should be considered. It relies on theoretical results of asymptotic discrete geometry. A direct consequence is the automatic detection of the noisy or damaged parts of the contour, together with its quantitative evaluation (or *noise level*). Apart from a given maximal observation scale, the proposed approach does not require any parameter tuning and is easy to implement. We demonstrate its effectiveness on several datasets. We present different direct applications of this local measure to contour smoothing and geometric estimators whose algorithms initially required a noise/scale parameter to tune: They show the pertinence of the proposed measure for digital shape analysis and reconstruction.

Index Terms—Local noise detection, discrete geometry, maximal segments, shape analysis

1 INTRODUCTION

THE geometric analysis of discrete or digital contours is of primary importance for shape recognition or shape matching. Discrete contours that arise naturally from digitization processes or from image segmentation algorithms are by nature nonsmooth and their geometric analysis requires specific approaches. Examples of such approaches can be found in the discrete geometry field, where the most accurate techniques generally rely on the extraction of *maximal segments*, which are local affine reconstruction of contours.

In most cases, digital contours are not perfect digitizations of ideal shapes but present noise and perturbations. This is also true for regions produced by most segmentation algorithms, whose regularizers penalize length but not curvature. Rather recently, *blurred segments* were introduced to take into account both the discreteness and possible noise of data [1]. They are parameterized with a value related to the thickness of the perturbation. Based on this, discrete tangent and curvature estimators robust to noise have been developed [2], [3]. Similarly, the curvature estimator of [4] requires a smoothing parameter related to the amount of noise. In pattern recognition too, many techniques for

extracting feature points, dominant points, or corners rely on one or more external parameters that are determinant for removing contour perturbations due to noise (e.g., see [5]).

Two factors limit the applicability of these techniques: First, their parameterization requires a user supervision, second, this parameter is global to the shape, while the amount of noise may be variable along the shape.

Strangely enough, this issue has not been tackled in the discrete geometry and pattern recognition communities. However, the similar problem of noise detection and appraisal in gray-level or color images has been studied a lot in the image processing and edge detection community. It has led to the development of multiscale analysis [7], [8]. In a way, noise detection is postponed to a later process which will analyze the scale-space instead of the image. Further improvements lead to the automatic determination of a local scale, whose aim is either to improve edge detection or image restoration. Some approaches rely on a global optimization scheme, like the one of Jeong and Kim [9]. Its optimization is, however, difficult. The Mumford-Shah model of image segmentation [10] is also a global technique for getting rid of the noise by fitting a piecewise continuous function. However, the delineated regions may have perturbed boundaries. The noise removal algorithm based on nonlinear total variation by Rudin et al. [6] is efficient to remove a global Gaussian noise of known characteristics. As illustrated in Fig. 1, this approach is less convincing for binary images with variable noise. Along the same lines, global approaches like morphological operations (see Fig. 1) or Gaussian smoothing failed at preserving features and removing noise at the same time.

Most methods adopt a local optimization procedure for finding the best local scale. Elder and Zucker [11] determine the minimum reliable scale by fitting a blurred step-model of

• B. Kerautret is with LORIA UMR CNRS 7503, Campus Scientifique, University of Lorraine, BP 239, 54506 Vandoeuvre-lès-Nancy Cedex, France. E-mail: kerautre@loria.fr.

• J.-O. Lachaud is with the Laboratoire de Mathématiques (LAMA), UMR CNRS 5127, UFR SFA, Campus Scientifique, University of Savoie, 73776 Le Bourget-du-Lac Cedex, France.

E-mail: jacques-olivier.lachaud@univ-savoie.fr.

Manuscript received 27 May 2011; revised 30 Dec. 2011; accepted 8 Jan. 2012; published online 19 Jan. 2012.

Recommended for acceptance by J. Jia.

For information on obtaining reprints of this article, please send e-mail to: tpami@computer.org, and reference IEEECS Log Number TPAMI-2011-05-0339.

Digital Object Identifier no. 10.1109/TPAMI.2012.38.

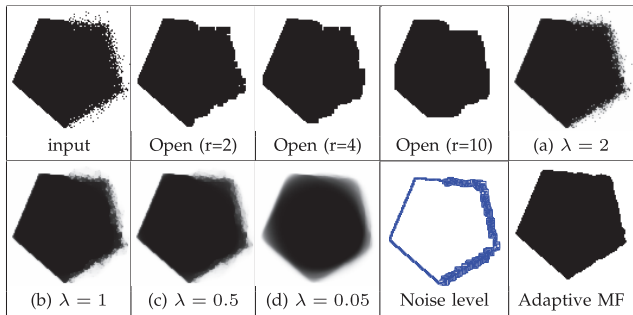


Fig. 1. Top row: Partially damaged input image and results of morphological operations. Images (a)-(d): Noise removal algorithm of Rudin et al. [6]. The parameter λ controlling the noise removal is global to the image. Removing significant noise induces a general smoothing. Our noise detection algorithm (bottom, second from right) could provide interesting information to such algorithms. An adaptive median filter using this information (see Section 5) creates the image at bottom right.

a contour. Kervrann [12] proposes to determine the best local window for a local piecewise constant reconstruction of the image by a statistical method. Many other approaches are related to anisotropic diffusion [13] and nonlinear filtering [14]. They aim at defining locally what the threshold between diffusion and sharpening should be. Among them, we quote the work of Chen [15], which uses a local discontinuity measure to constrain the anisotropic diffusion, and the work of Goshtasby and Satter [16], which smoothes images according to adaptive windows depending on the local image gradient structure.

Although very interesting for image processing, these techniques cannot be used to process binary images or, equivalently, segmented region boundaries and digital contours. They indeed rely either on a local SNR analysis of the image, sometimes with a user-given global SNR parameter, or on gradient information. Since we have only the discrete contour as input, both types of information are not computable.

We propose here a new method for estimating locally if the digital contour is damaged, what the amount of perturbation is, and what the meaningful scales are at which this part of the contour should be considered. Our method is similar in spirit to multiscale analysis, but relies on specific properties of digital contours. We indeed know several asymptotic properties of *perfect shape digitizations*. The main idea is to look for these asymptotic properties in the multiresolution decomposition of the given contour. If they are present, then the scale is meaningful; otherwise the contour is still noisy at this scale and must be examined at a coarser scale. Our approach is local, requires no parameter tuning (except a given maximal observation scale), and is easy to implement. Its output can be used in many applications which require a global or local noise parameterization. Among them, we may quote tangent or curvature estimators, dominant point, and corner detection.

In Section 2, we recall standard notions of discrete geometry and known asymptotic results concerning maximal segments defined along the contour of shape digitizations. We show that the length of maximal segments over scales can be used both to distinguish between flat and curved parts of a contour and to detect noise. These characteristics are to be found in the *multiscale profile* of each point of the digital contour. We present how to compute

them from the subsamplings of the input contour. Section 3 gives several ways for interpreting the multiscale profile of a point, depending on whether the user wishes to detect the first local reliable scale (*meaningful scale, noise level*) or the finest local reliable scale knowing a global coarse reliable scale (*standard scale*). In Section 4, we validate our technique on several datasets containing different shape geometries, localized and/or variable noise, various resolutions. All datasets are processed uniformly without any specific parameterization. Noise and reliable scales are correctly determined and quantified in all cases. Since the method is based on the expected object geometry and not on a particular noise model, the resulting noise detection appears able to process various types of noise (even if it could exist particular noise models not detected by our method). Our noise quantifier is also shown to be globally consistent since it keeps the same response along the digital shape contour for a stationary noise whatever the chosen resolution. We further demonstrate the potential of our approach in Section 5, where we give four straightforward applications of our noise detector. The first one is the simple adaptive median filtering of the digital object according to its noise level: Sharp features are preserved while noise is removed. The second one is the local parameterization of a discrete tangent estimator [17]. Tangent estimation is improved in damaged regions while its precision is preserved in undamaged parts. The third one is the exploitation of detected noise level for the parameterization of two classical contour reconstruction algorithms [18], [19]. The fourth one is the evaluation of the segmentation accuracy of the power watershed algorithm [20]. Section 6 presents some perspectives to this work. The presented noise detector is available online at [21].

2 MULTISCALE PROPERTIES OF MAXIMAL SEGMENTS

2.1 Definition and Known Asymptotic Results

Introduced in the 1970s, digital straightness has been an active research subject through many years (e.g., [22], [23], [24], and [25] for a recent review). In this paper, we consider the following definition.

A *standard Digital Straight Line (DSL)* is some set $\{(x, y) \in \mathbb{Z}^2, \mu \leq ax - by < \mu + |a| + |b|\}$, where (a, b, μ) are also integers and $\gcd(a, b) = 1$. The real lines of equation $ax - by = \mu$ and $ax - by = \mu + |a| + |b|$ are, respectively, the lower and upper leaning lines (as illustrated in the next floating figure). It is well known that a DSL is a 4-connected simple path in the digital plane. A *Digital Straight Segment (DSS)* is a 4-connected piece of DSL. The interpixel contour of a simple digital shape is a 4-connected closed path without self-intersections. Given such a 4-connected path C , a *maximal segment* M is a subset of C that is a DSS and which is no more a DSS when adding any other point of $C \setminus M$.

The following floating figure illustrates a recognition process of a maximal straight segment initiated from the point P_0 (like the recognition algorithm of Debled Rennesson and Reveilles [26]). From this point the sequence $P_1, P_{-1}, P_2, P_{-2}, P_3, P_{-3}, P_4, P_{-4}, P_5, P_{-5}, P_6, P_{-6}, P_7, P_{-7}, P_8, P_{-8}, P_9$ is added alternately to the front and to the back of the current segment. The final segment is maximal since the points P_{-10} and P_6 cannot be added. The resulting recognition process

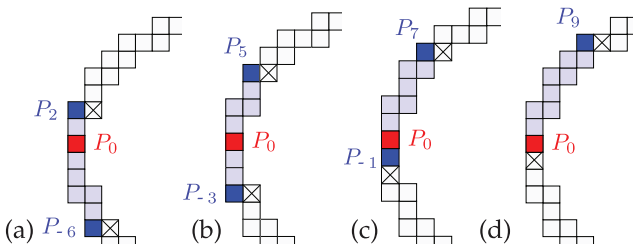
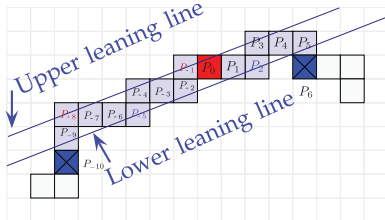


Fig. 2. Illustration of the set of all maximal DSS covering a discrete point P_0 with discrete lengths L equals, respectively, to 8, 8, 8, and 9.

gives also the DSS characteristics $(a, b, \mu) = (2, 5, 0)$ and its discrete length $L = 14$ which is simply defined as its number of pixels minus one.



A discrete contour point can be covered by several maximal DSS. For instance, the point P_0 of Fig. 2 is covered by four DSS (a)-(d). Note that the set of all maximal DSS can be computed in linear time according to the contour size [17]. Such a detection can be done by removing points from the back of the DSS and by adding new points to the front. For instance, from the DSS (a) of Fig. 2, the DSS (b) is obtained by removing the point P_{-6}, P_{-5}, P_{-4} and by adding P_3, P_4 , and P_5 . In the following, we will denote by L_j the length of the j th DSS covering a point P . As an example, the notation L_3 will denote the length of the third DSS which cover P_0 on Fig. 2c.

We recall some asymptotic results related to maximal segments that lie on the boundary of some shape X digitized with step h . The digitization process is $\text{Dig}_h(X) = X \cap h\mathbb{Z} \times h\mathbb{Z}$ (Gauss digitization [27]). First, we assume the shape has smooth C^3 -boundary and is strictly convex (no flat zones, no inflection point). Lachaud [28, Theorem 5.26] states that the smallest discrete length—the number of pixels minus one—of the maximal segments on the boundary of $\text{Dig}_h(X)$ is some $\Omega(1/h^{1/3})$. The longest discrete length of the maximal segments on the boundary of $\text{Dig}_h(X)$ is some $O(1/h^{1/2})$ function ([17, Lemma 15]). Fig. 3 presents experimental measures of the DSS length obtained on the digitizations of a circle. The discrete minimal, maximal, and average length fit the theoretical behavior defined from the previous theorem well.

Second, we observe maximal segments along the digitization of a flat zone of a shape. Since digital straight segments are digitization of straight line segments, there is at least one maximal segment that covers the straight line. It means that the discrete length of the longest maximal segment is $\Theta(1/h)$.

As a corollary to the previous properties, by considering not only strictly concave or convex shape we obtain:

Corollary 1. Let S be a simply connected shape in \mathbb{R}^2 with a piecewise C^3 boundary. Let P be a point of the boundary ∂S of S . Consider now an open connected neighborhood U of P on

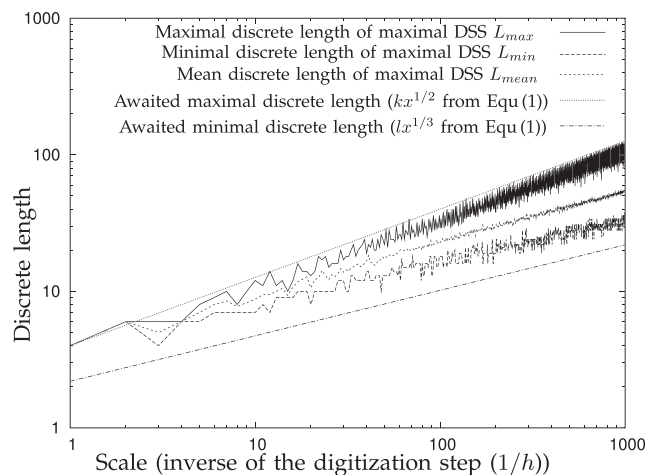


Fig. 3. Illustration of the asymptotic behavior of the discrete length of maximal discrete straight segment on a circle of radius 1. The abscissa represents the inverse of the digitization step h . The upper and lower bound from (1) are plotted as a reference for illustration with chosen values of k and l .

∂S . Let (L_j^h) be the discrete lengths of the maximal segments covering P along the boundary of $\text{Dig}_h(S)$. Then, if U is strictly convex or concave, then

$$\Omega(1/h^{1/3}) \leq L_j^h \leq O(1/h^{1/2}). \quad (1)$$

U has null curvature everywhere, then

$$\Omega(1/h) \leq L_j^h \leq O(1/h). \quad (2)$$

The first inequality expresses the asymptotic behavior of the length of maximal segments in smooth curved parts of a shape boundary. The second one gives the analog properties in flat parts of a shape boundary.

2.2 From Asymptotic to Scale Analysis by Subsampling

In the context of image analysis and pattern recognition, we do not have access to asymptotic digitizations of shapes: We are not able to get finer and finer versions of the object. At first glance, it could mean that asymptotic properties are not useful to analyze shape boundaries. This is not true. We can use asymptotic properties in a reverse manner. We consider that our digital object D is the digitization of some euclidean shape X at a grid step h , choosing, for instance, the Gauss digitization again. We then subsample the digital object D with covering “pixels” of increasing sizes $i \times i$, for $i = 2, 3, \dots, n$. The subsampling process ϕ_i will be described in Section 2.3. The family \mathcal{D} of digital objects $\phi_n(D), \dots, \phi_2(D), D$ is an approximation of a sequence of finer and finer digitized versions of X , namely, the family $\mathcal{X}: \text{Dig}_{nh}(X), \dots, \text{Dig}_{2h}(X), \text{Dig}_h(X)$. Corollary 1 holds for the latter family \mathcal{X} . Although this corollary does not formally hold for the family \mathcal{D} , a similar behavior is observed in practice (see, for instance, the plots of points P_1 and P'_1 from Figs. 5b and 5d or the complementary experiments from the annex, part A [29]).

When looking at lengths of maximal segments around some point P of the boundary of D , we should thus observe a decreasing sequence of lengths for the increasing sequence of digitization grid steps $h_i = ih$, whose slope is

related to the fact that P was in a flat or curved region. More precisely, letting $(L_j^{h_i})_{j=1 \dots l_i}$ be the discrete lengths of the maximal segments along the boundary of $\phi_i(D)$ and covering P , we can expect:

- If P is in a curved convex or concave zone, then the lengths $L_j^{h_i}$ follow (1).
- If P is in a flat zone, then the lengths $L_j^{h_i}$ follow (2).

The asymptotic bounds of these equations suggest:

Property 1 (Multiscale). *The plots of the lengths $L_j^{h_i}$ in log-scale should be approximately affine with negative slopes as specified below:*

plot	expected slope (curved part)	expected slope (flat part)
$(\log(i), \log(\max_{j=1 \dots l_i} L_j^{h_i}))$	$\approx -\frac{1}{2}$	≈ -1
$(\log(i), \log(\min_{j=1 \dots l_i} L_j^{h_i}))$	$\approx -\frac{1}{3}$	≈ -1

The plot is only approximately affine since the preceding properties are asymptotic. Given an object at a finite resolution, subsampling induces length variations that only approximately follow the asymptotic behavior. Arithmetic artifacts also play a role in this. It is, however, clear that the approximation gets better when the initial shape is digitized with a finer resolution.

We can make several remarks about the preceding result. First, it allows us to distinguish between flat parts and curved parts of an object boundary, provided the object was digitized with a reasonable precision. This distinction relies only on the classification of the plot slope between $[-1, -1/2]$ and $[-1/2, -1/3]$. Second, the preceding approach is not valid on (around) points that are 1) a transition between a flat and a curved part, 2) corner points. Third, this technique assumes smooth objects with perfect digitization: If the digital contour has been damaged by noise or digitization artifacts, these characterizations do not hold.

Although the two last remarks seem problematic for analyzing shapes, we will use them to *locally* detect the amount of noise and to extract *local* meaningful scales.

2.3 Subsampling a Digital Contour

Our multiscale analysis of digital contours requires several subsampling computations of the initial digital shape. The subsampling as selected in our approach is not spatial but operates along the digital contour [30]. The output subsampled contour is denoted by $\phi_i^{x_0, y_0}(C)$, where x_0 and y_0 is the shift needed for the subsampling (with $0 \leq x_0, y_0 < i$). The index correspondence between points along the two contours is computed during the subsampling. Along with $\phi_i^{x_0, y_0}(C)$, there is thus a surjective map $f_i^{x_0, y_0}$ which associates any point P in C to its image point in the subsampled contour $\phi_i^{x_0, y_0}(C)$. Several subsampled contours are illustrated on Figs. 4a, 4b, and 4c and the map $f_3^{0,0}$ is shown in Fig. 4d. This subsampling similar to the common spatial one, can be done either locally around the point of interest or globally for the whole contour.

2.4 Local Geometric Evaluation with Multiscale Criterion

We are now in a position to analyze the local geometry of some point P on a digital contour C . For resolution i and a

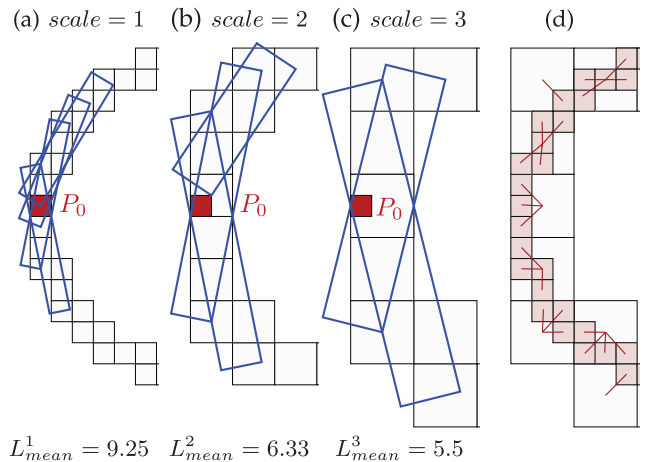


Fig. 4. Illustration of the set of maximal segments covering a point P at different scales (a)-(c). L_{mean}^s gives the mean discrete length of the DSS covering P at scale s . (d) shows the function (represented by lines) associating each pixel P of C to the point $\phi_3^{0,0}(P)$.

shift (x_0, y_0) , we compute the discrete lengths $L_j^{h_i, x_0, y_0}$ of the maximal segments of $\phi_i^{x_0, y_0}(C)$ containing $f_i^{x_0, y_0}(P)$. To take into account the possible digitization artifacts and approximations, we average these lengths as

$$\bar{L}^{h_i} = \frac{1}{i^2} \sum_{0 \leq x_0 < i, 0 \leq y_0 < i} \frac{1}{l_i^{x_0, y_0}} \sum_j L_j^{h_i, x_0, y_0},$$

where $l_i^{x_0, y_0}$ represents the number of maximal segments containing $f_i^{x_0, y_0}(P)$. As previously described in Section 2.1, all the maximal segments of $\phi_i^{x_0, y_0}$ can be computed in linear time with the number of points [17]. Fig. 4 illustrates for a point P the cover of maximal DSS obtained at several scales with shift values $(x_0, y_0) = (0, 0)$.

The *multiscale profile* $\mathcal{P}_n(P)$ of a point P on the boundary of a digital object D is the sequence of samples $(\log(i), \log(\bar{L}^{h_i})_{i=1 \dots n})$. According to Property 1, these samples should be correctly approached with an affine model. Several examples of multiscale profiles are illustrated in Figs. 5b and 5d. We thus define the *ideal multiscale criterion* $\mu_n(P)$ of a point P on the boundary of a digital object D as the slope coefficient of the simple linear regression of $\mathcal{P}_n(P)$ (in the order regressor, regressand). An example of ideal multiscale criterion along a digital spiral is illustrated on Figs. 5e and 5f.

The slope defined by the ideal multiscale criteria $\mu_n(P)$ appears useful to detect the flat or concave/convex contour parts. In fact, Property 1 indicates that $\mu_n(P)$ should be around -1 if P is in a flat zone, whereas it should be within $[-1/2, -1/3]$ if P is in a strictly convex or concave zone. A complementary study [31] and others experiments [30] have shown that this distinction can be reasonably performed by using a threshold (denoted as $t_{f/c}$) set around to -0.52 .

3 MULTISCALE PROFILE ANALYSIS

There are several ways to analyze the resulting multiscale profile defined in the previous section. The first one is to detect the first local scale for which the contour part can be considered as meaningful: It naturally induces a noise level definition. The second one is to start from a global coarse scale and to detect the finest reliable scale (*standard scale*).

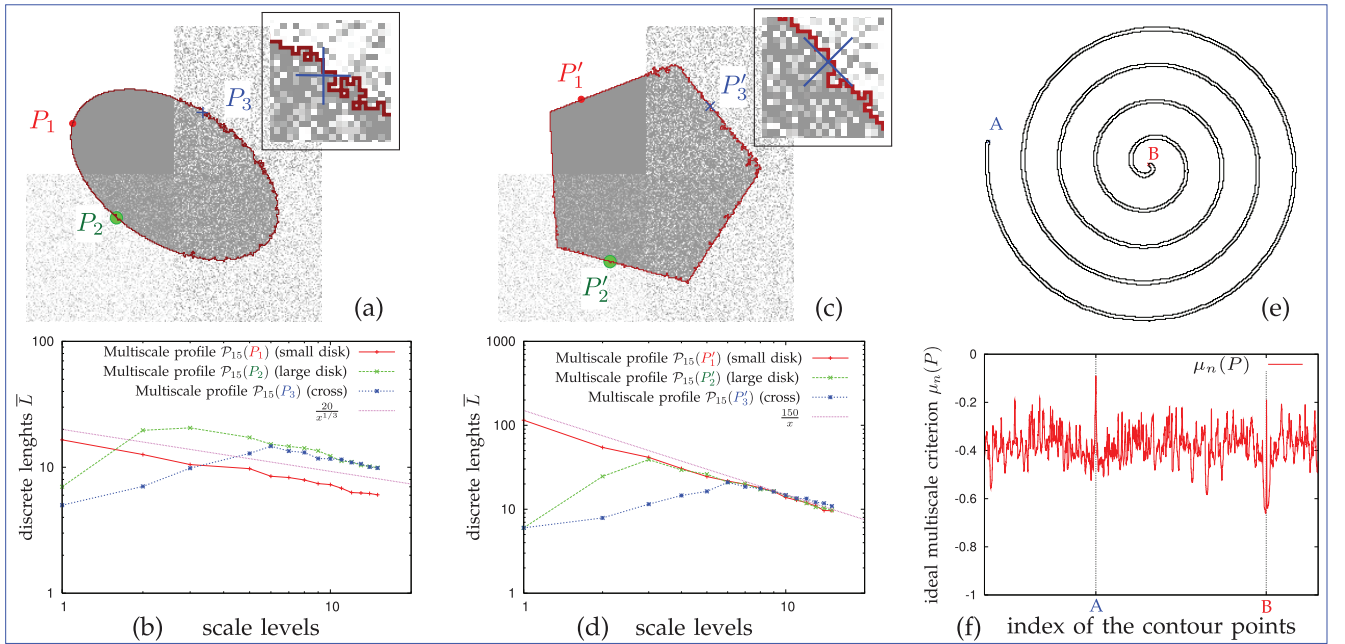


Fig. 5. Examples of multiscale profiles (a)-(d) and illustration of the *ideal multiscale criterion* $\mu_n(P)$ on a spiral (e) and (f). (a) and (b) show examples of multiscale profiles $\mathcal{P}_{15}(P)$ on ellipse: P_1 in a curved zone, P_2 in a slightly perturbed curved zone, P_3 in a strongly perturbed curved zone. Gaussian noise (source image illustrated in the background in light gray) was added on each area containing the point P_1 , P_2 , and P_3 with, respectively, the following standard deviation $\sigma_1 = 0$, $\sigma_2 = 75$, and $\sigma_3 = 175$. The same experiment is applied on the polygon (c) and (d) with the points P'_1 , P'_2 , and P'_3 .

3.1 Meaningful Scales and Noise Detection

The multiscale profile can be used to detect noisy digital contours. Indeed, if the multiscale profile of some point P is not some approximation of an affine map with negative slope, it means that locally around P the shape geometry is neither a flat or curved zone. We display in Figs. 5a and 5b the multiscale profile of a point P_1 located on a perfectly digitized curved zone and the multiscale profiles of the points P_2 and P_3 located in noisy zones. In the former profile, the decreasing affine relation is immediately visible. In the latter profiles, it is somewhat randomly increasing for fine resolutions and then follows an expected decreasing affine profile after a given scale. A similar behavior is observable for the multiscale profiles on the pentagon shape with similar noisy regions. The only difference is the slope of the affine relation of the profiles (slopes near $-\frac{1}{3}$ for the plots of Fig. 5b and near -1 for the plots of Fig. 5d).

We, therefore, introduce a *noise threshold* t_m to discriminate between a curved zone and a noisy zone. From this parameter a *meaningful scale* of a multiscale profile $(X_i, Y_i)_{1 \leq i \leq n}$ is then defined as a pair (i_1, i_2) , $1 \leq i_1 < i_2 \leq n$, such that for all i , $i_1 \leq i < i_2$, $\frac{Y_{i+1}-Y_i}{X_{i+1}-X_i} \leq t_m$, and the preceding property is not true for $i_1 - 1$ and i_2 . According to the analysis and experiments of [30] it appears that the threshold $t_m = 0$ gives locally precise noise detection both on curved or flat zones and near corners. Note that setting parameter t_m between $-1/3$ and $1/3$ only slightly changes the noise detection, as shown in part B of the annex [29].

If (i_1, i_2) is a meaningful scale of the profile $\mathcal{P}_n(P)$, the (i_1, i_2) -multiscale criterion $\mu_{i_1, i_2}(P)$ of point P is then the slope coefficient of the simple linear regression of $\mathcal{P}_n(P)$ restricted to its samples from i_1 to i_2 .

Obviously, meaningful scales of $\mathcal{P}_n(P)$ do not overlap and are thus naturally ordered. If the first meaningful scale

of $\mathcal{P}_n(P)$ is (k_1, k_2) , then the integer $k_1 - 1$ is called the *noise level* at point P and we denote it by $\nu(P)$.

We will show in the experiment section that both definitions of meaningful scales and noise level have a clear intuitive interpretation. They determine precisely where the contour is perturbed and how it should be interpreted to be meaningful.

3.2 Standard Scale

In presence of a large amount of noise (or for the special case of fractal shapes) the first meaningful scale is not always relevant compared to the global shape. For example, if we consider the shape of Fig. 6a we can see that the first meaningful scale of the point represented by a cross indicates a zero noise level while the noise is well visible from a global point of view: This phenomenon appears in places where the noise is so important that its geometry becomes pertinent at small scales. In order to detect the global shape scale we propose another strategy by defining the *standard scale*. This strategy is *top-down* and assumes that

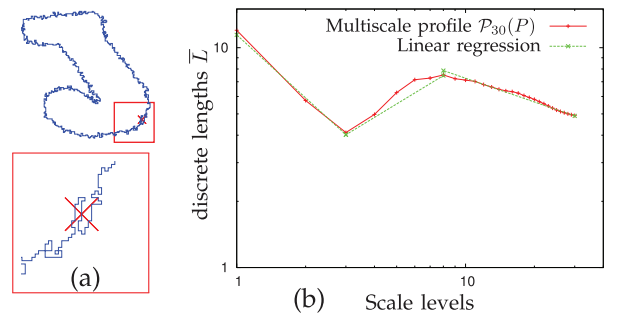


Fig. 6. Illustration of standard scale on a noisy contour. The standard scale of the point represented by a cross is equal to $(8, 30)$.

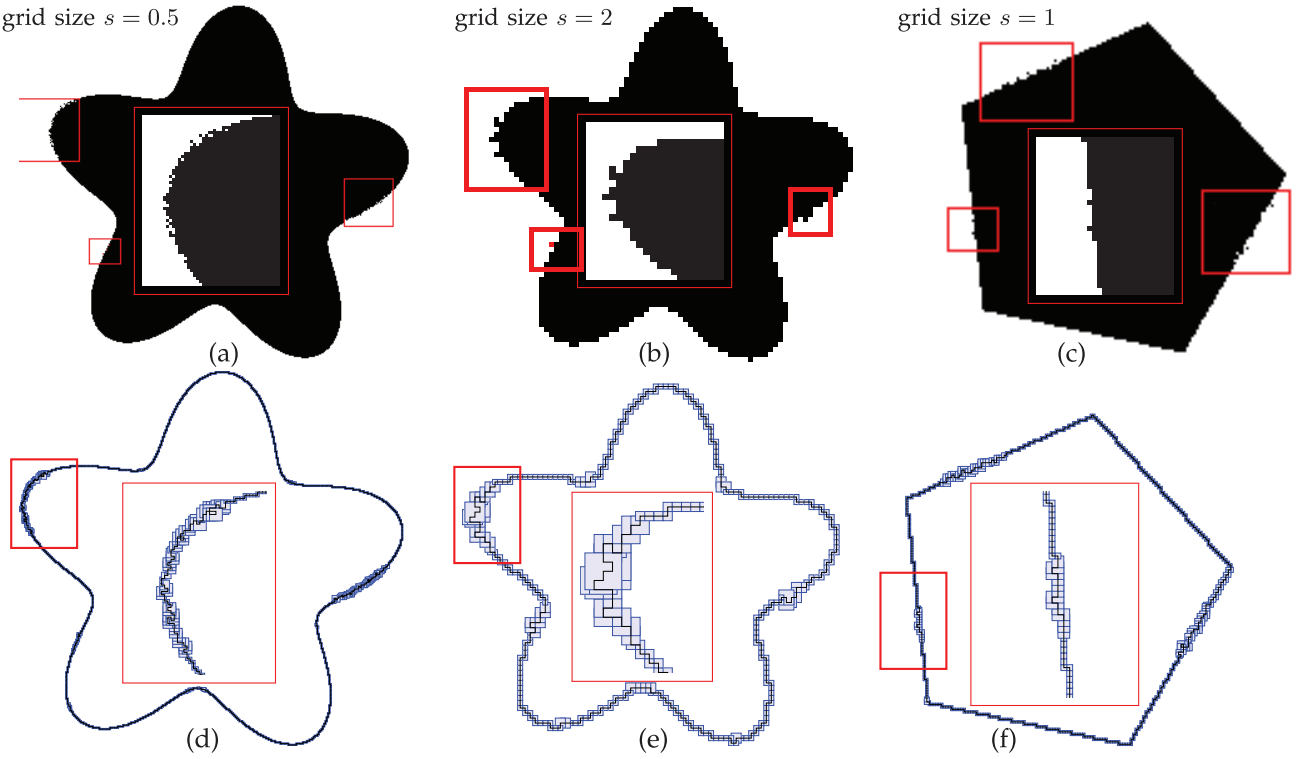


Fig. 7. Noise detection on flower-like and polygonal shapes defined with several grid sizes (s). Noisy areas are highlighted by red boxes (images (a)-(c)) and were obtained after adding locally Gaussian noise or by manually editing some single pixel values (b) and (c). The areas outside boxes are not changed from the initial reference shape. The resulting noise detection is shown in (d)-(f) by displaying for each pixel P a centered box of size $\nu(P) + 1$.

the parameter n gives a coarse scale at which the whole shape is relevant.

This notion is defined from the decomposition of the multiscale profile $(X_i, Y_i)_{1 \leq i \leq n}$ into a sequence S_k of k pairs $(i_1, i_2), (i_2, i_3), \dots, (i_k, i_{k+1})$, $1 \leq i_k < n$ and $i_{k+1} = n$, each of them corresponding to the linear regression computed by starting from highest index i_{j+1} to i_j , $1 \leq j \leq k$, and which is false for $i_j - 1$. The linear regression model was used with a confidence rate set empirically to 70 percent after experiments on various contours. The slope of the linear regression between i_j and i_{j+1} is denoted by θ_{i_j} . From this profile decomposition the standard scale is defined as the first interval (i_l, i_m) , $1 \leq l < m \leq k + 1$, computed starting from scale n such that for all p , $l \leq p < m$, $\theta_{i_p} < 0$, and such that $\theta_{i_{l-1}} \geq 0$ or $i_l = 1$. The integer i_l defines the standard scale level of the point P and is denoted by $\sigma(P)$.

Fig. 6 illustrates the standard scale obtained on a noisy contour point. The point on Fig. 6a has zero-level noise according to its meaningful scale, while it presents a large noise level of 7 according to its standard scale equal to $(8, 30)$.

4 EXPERIMENTAL VALIDATION

4.1 Noise Detection

A robust noise detector should not detect noise on perfectly digitized data and should not be sensitive to the object initial resolution. To experiment with these properties, different shapes have been generated with a manual addition of noise (Gaussian or manually added by edition) on some specific areas (see Fig. 7). Note that for certain areas (on the bottom left of the shape) only one or three pixels were changed (highlighted in red). For each pixel P of the contour, the

result of the noise detection is illustrated by drawing a box of size $\nu(P) + 1$, i.e., its first meaningful scale.

The obtained noise detection displayed on Figs. 7d, 7e, and 7f shows good precision. Even with low resolution shapes and with a one pixel change, the noise is detected well. Only a few false positive noise detections can be seen on some small areas on the flower (near corners): However, these errors are limited to one noise level. Note that for all of these experiments no parameter was changed for the detection. The variable t_m associated to the noise threshold was set to 0 for all the experiments, as suggested in Section 3.1. The maximal resolution n used in the definition of the multiscale profile $\mathcal{P}_n(P)$ only has an influence on the maximum scale of the detected noise. Indeed, for example, the use of the minimal value of $n = 2$ induces a noise detection only at scales 1 and 2. This value was set to 15 in all the presented experiments.

4.2 Global Noise Detection on Several Grid Sizes

The behavior of noise detection with respect to different object sizes or samplings was analyzed by generating noisy shapes with several grid sizes. We used a noise model defined by a power law similar to the noise model proposed by Kanungo [32]. The probability P_d of changing a pixel located at a distance d from the shape boundary is defined as $P_d = \frac{a}{b^d}$. The parameters were set in order to take into account the grid size s , $a = \frac{1}{2^s}$, and $b = 2$. The generated noisy shapes are illustrated in Figs. 8a, 8b, 8c, and 8d. The resulting noise level estimation shows a mean value approximately near size 5 (according to an initial grid size s equals to one) for the two types of shapes (circle and polygon) and for all grid sizes (graphics (e) and (f) of Fig. 8).

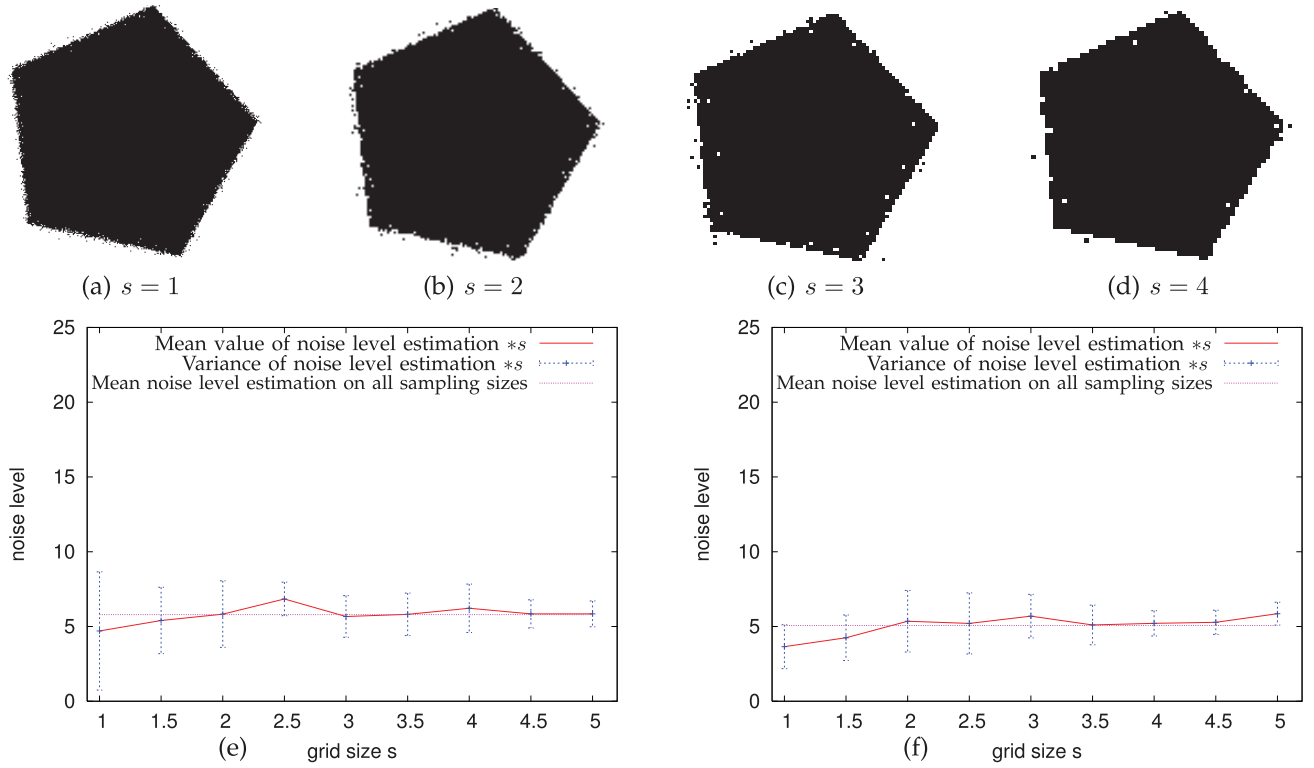


Fig. 8. Global noise detection on several grid sizes s . Shapes (a)-(d) were obtained with the Kanungo noise model [32] defined on each grid size s (i.e., the amount of noise is independent of the sampling resolution). Plots (e) and (f) show the noise level estimation obtained on a pentagon (e) and on a circle (f) of radius 120 with a sampling grid size s varying from 1 to 5.

This demonstrates the ability of the proposed approach to automatically detect the real noise scale, independently from the object sampling.

4.3 Detection of Flat and Curved Contour Areas

As described in the previous section, the analysis of the multiscale profile $\mathcal{P}_n(P)$ can discriminate the curved and flat areas of the contour. In order to take into account only the significant part of the profile of a point P , we use the (i_1, i_2) -multiscale criterion ($\mu_{i_1, i_2}(P)$) which defines the slope of the profile only from the meaningful scale (i_1, i_2) . From this value, the decision curved/flat relies on a constant threshold value $t_{f/e}$, which is set to -0.52 to maximize the good detection as suggested in Section 2.4.

The detection experiment was conducted on both perfect and noisy shapes with exactly the same parameters. Figs. 9a, 9b, and 9c shows the results obtained on perfectly digitized shapes composed of various curved and flat parts. The detection is accurate everywhere except on a few small areas (Fig. 9b), which are not detected as curve in some parts of the spiral (related to octant changes). On the damaged shapes Figs. 9e-9g, the detection is always fine and looks insensitive to the different noise intensities.

4.4 Experiments on Real Images

Our method was applied on real images with unchanged parameters (Fig. 10). Contours were defined by tracking the border of the regions obtained by thresholding the grayscale image. The image of Fig. 10a was directly extracted without subsampling from a digital camera picture obtained at resolution $4,000 \times 2,672$ with a sensibility of 250 ISO. As for the previous experiments, the detected noise level K of a

point P is illustrated by drawing a box of size K centered on each point P (Figs. 10b-10d). These results are comparable to the ones obtained on synthetic images. In the same way, the curved part detection was performed on the shapes of Fig. 10d. As previously, the main curved parts of the characters are well detected (represented by large blue (dark) pixels in Fig. 10e). Other experiments on contours extracted from real images (Figs. 9d and 9h) also show good detections.

By considering the global contour of Fig. 10b one could expect a noise level at a greater scale than the one obtained with the meaningful scale detection. As suggested in Section 3.2 we instead apply the standard scale detection. Fig. 11a shows that the top-down strategy of the standard scale is a better choice in this case and Fig. 11b gives the reconstructed digital contour obtained from the standard scale measures (see also Section 5.1).

4.5 Meaningful Level Set

Experiments on grayscale image can also be done by extracting the digital contours from level sets defined by successive thresholds of the image gray levels (and by using a border tracking algorithm on the thresholded connected components). Fig. 12b illustrates the 50,692 contours obtained with a threshold step equals to 10. The meaningful contour parts are defined as the set of points P for which the first meaningful scale $\nu(P)$ is one and such that P is not included in the neighborhood of size $\nu(Q) > 1$ of another contour point Q . More precisely, if we denote by $S_{i,j}$ the sequence of points of the contour C going

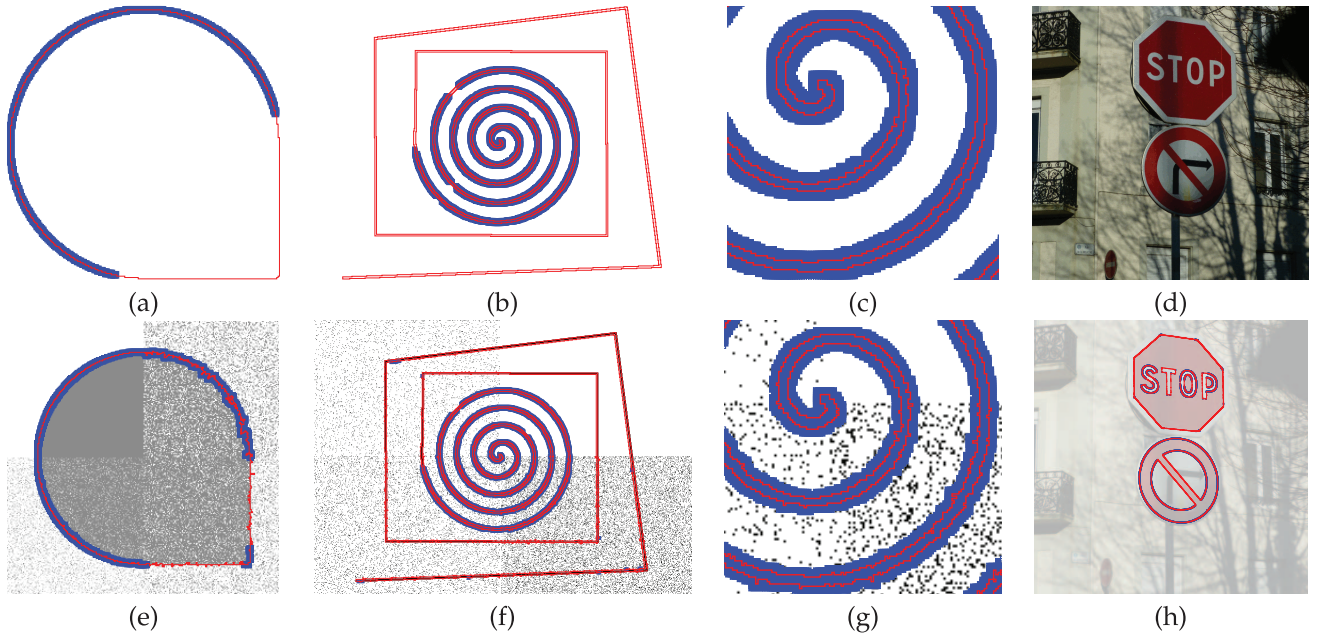


Fig. 9. Detection of flat/curved areas on various shapes using the meaningful scales information. The large blue pixels (in dark) represent the detected curved areas. Images (e)-(g) are the noisy version of the shapes represented in images (a)-(c). The noisy versions of (a) and (b) were obtained by applying noise specifically on the quadrants of the image as used for Figs. 5a and 5c) (illustrated in the background in light gray). (c) and (g) are, respectively, the close-up view of the center area of images (b) and (f). (h) shows the results obtained on the segmentation of image (d). All these results were obtained with a maximal allowed scale set to 25 (it was increased since the images have a larger resolution).

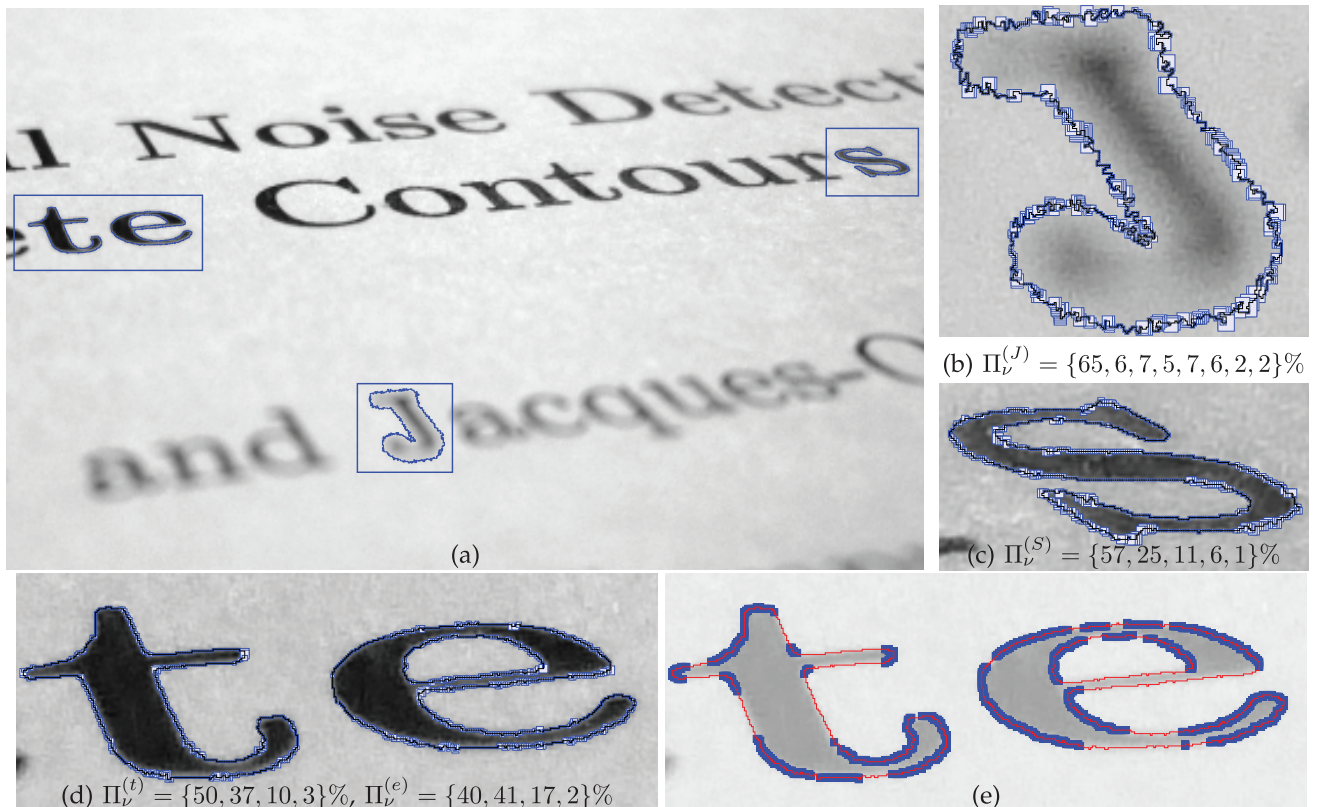


Fig. 10. Noise (b)-(d) and curved parts (e) detection applied on real text photography (a). The contours of the characters were extracted by thresholding the gray level image and by tracking the resulting connected component border. Noise is represented by light blue boxes (of size $\nu(P) + 1$) in images (b)-(d), while curved parts are highlighted with large dark blue boxes in image (e). The noise partition $\Pi_{\nu}^{(X)}$ gives, for each shape X , the percentage c_i of points P having for noise level $\nu(P) = i$, i.e., $\Pi_{\nu}^{(X)} = \{c_0, c_1, \dots, c_i, \dots, c_k\}$.

increasingly from point $P_{min(i,j)}$ to $P_{max(i,j)}$ included, its meaningful parts are defined as the set $\{P \in C \setminus \{P \in C | \nu(P) > 1\} \cup \{P_i \in C | \exists k | \forall P_l \in S_{k,i}, \nu(P_k) \geq \|P_k P_l\|\}\}$. The

resulting meaningful contours parts are well visible on Fig. 12c while the flat meaningful parts are also well detected on Fig. 12d.

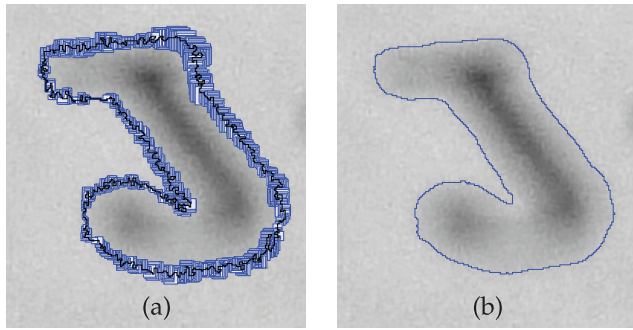


Fig. 11. Illustration of the standard scale levels σ (a). For each pixel P of the contour a centered box of size $\sigma(P)$ is displayed. Reconstruction from the standard scale median filter is displayed in (b).

4.6 Timing Measures

To conclude the experimentation part, some runtime measures were performed on the contours of Fig. 10. The runtimes listed in the following table were obtained on a 2.4 GHz Intel Core Duo. The measures include the computation of all subsampled contours $\phi_i^{x_0, y_0}(C)$ and their maximal segments.

nb points	226	702	788	874	1450
runtimes (ms)	178	363	387	411	513

5 APPLICATIONS

5.1 Contour Smoothing

Meaningful scales can be used to locally remove noise detected from the input shape. For instance, a simple application is to define an adaptively sized mask in a classical median filter [33]. To process such a filter, from a contour pixel P , we assign a mask size $K = 2\nu(P) + 1$ to all points contained in the neighborhood of size K centered in P . If several mask sizes are assigned to one pixel, the maximal mask size is retained.

This *meaningful scale median filter* (MS median filter) has been applied on the shapes of Figs. 7a, 7b, and 7c). The noise present in the initial shapes was removed well, as can be seen in Fig. 13. Moreover, the sharp features on the polygonal shapes are well preserved. In order to quantify the smoothing accuracy, we measure the number of pixels which differ from the original ideal image (not the corrupted input image). Table 1 shows the number of incorrect pixels with a comparison between the MS median filter and various constant size median filters. If we except shape "FlowerR1," the results obtained are always the best with the MS median filter.

Other comparisons were performed on a noisy star shape object. The initial star was damaged with various noise levels at several locations (see Fig. 14a). Fig. 14b shows its MS median filtering, which is very close to the original shape. When using a constant size median filter (Fig. 14c), small size masks are not enough to remove the noise, while large size masks remove the noise but provoke strong corner smoothing. Another denoising method specialized for processing binary document images [34] was also used for comparison (Fig. 14d). Similarly, a small value of the fidelity denoising parameter (ϵ) shows that noise is not

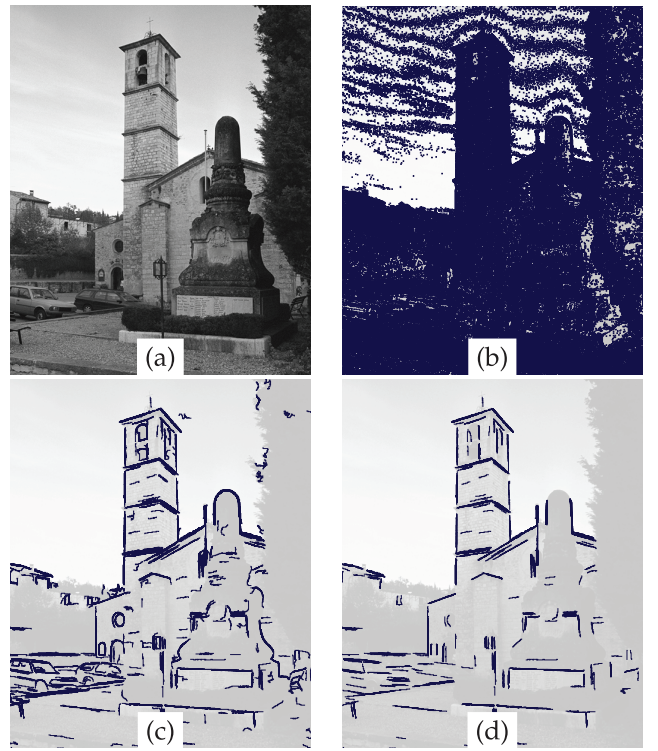


Fig. 12. Application on 50,692 level set contours (b) of the photograph of Valbone church (a). The contours were obtained after a threshold step equal to 10 from the 256 initial levels. Resulting meaningful contours (c) and flat contour parts (d).

removed everywhere and a larger value implies shape and corner enlargement.

The MS median filter was applied on the letters extracted from Fig. 10 and on a star obtained after a small rotation. As shown in Fig. 15, the parts with little noise are removed well, while smooth parts and corners without noise are preserved well. To extract the global contour of the noisy contour (b) of Fig. 10 we define the *standard scale median filter* by simply replacing the noise level $\nu(P)$ with the standard scale level $\sigma(P)$. The resulting contour presented in Fig. 11b shows the awaited contour representing the global shape without the very small variations visible at the finest scale.

A comparison between the MS median filter and the Markov Random Field (MRF) segmentation is illustrated in Fig. 16. Although the MRF is not limited to dealing with two classes segmentation problem, even by selecting a specific parameter β , the result of the MS median filter appears to fit the initial shape better. This filter can also be applied directly on the gray level image with the same isocontour. Such a restoration is illustrated in Fig. 17. The adaptive quality is well visible on the right image of the previous figure.

5.2 Geometric Analysis

Geometric estimators are generally sensitive to the amount of noise that may perturb the digital contour. This sensitivity can be reduced by choosing a scale parameter or by applying global noise reduction. Since meaningful scales appear useful in determining locally everywhere along the contour what the first relevant scale is, we experiment with it through

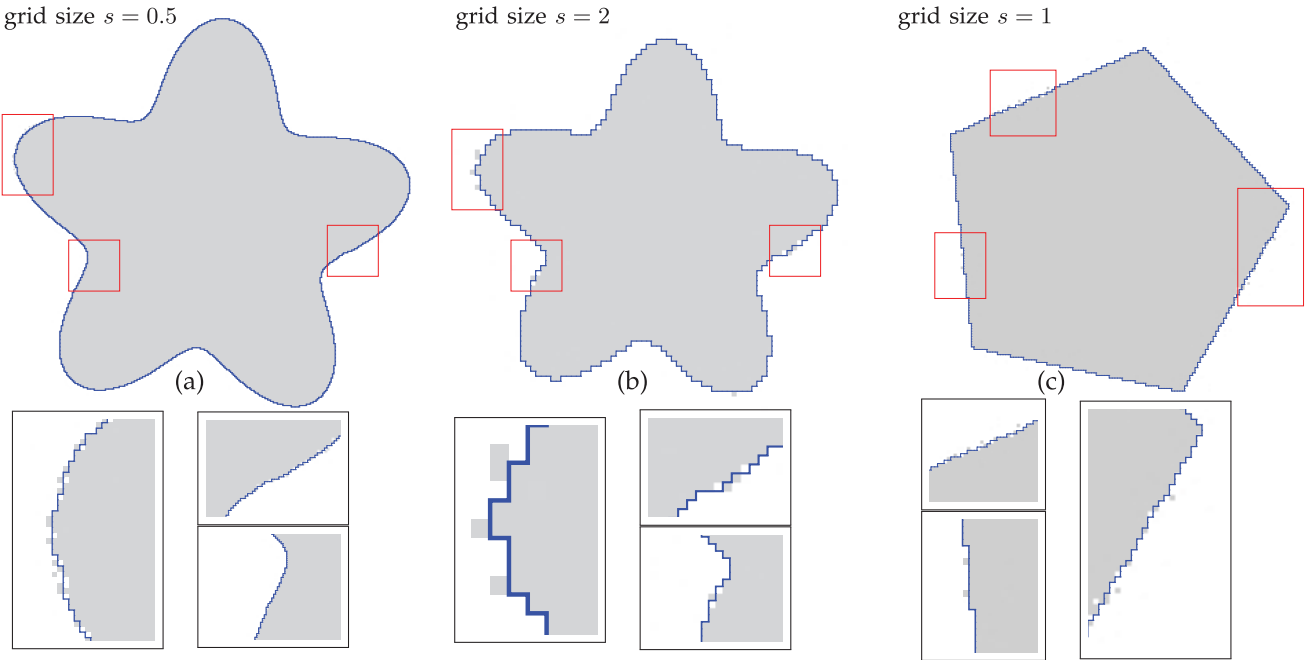


Fig. 13. Results obtained from the *meaningful scale median filter*. The initial shapes are represented in light gray and the resulting contour is shown in dark (blue color).

a digital tangent estimator based on maximal segments called λ -MST [17]. It has been shown to be one of the most accurate estimators for perfect shape digitizations.

The λ -MST estimator is based on the recognition of maximal segments along some discrete contour C , whose discrete points C_k are numbered consecutively. We denote by MS_i the maximal segments of the contour and by θ_i the angle they form with the x -axis. Each maximal segment MS_i is a 4-connected sequence of points of C going increasingly from point C_{m_i} to point C_{n_i} included. A pencil of maximal segments around some point C_k is defined as the set $\{MS_i, C_k \in MS_i\}$ and denoted by $\Gamma(k)$. The eccentricity $e_i(k)$ of a point C_k with respect to a maximal segment MS_i is its relative position between the extremities of MS_i :

$$e_i(k) = \begin{cases} \frac{\|C_k - C_{m_i}\|_1}{D_i} = \frac{k - m_i}{D_i}, & \text{if } MS_i \in \Gamma(k), \\ 0, & \text{otherwise,} \end{cases} \quad (3)$$

with $D_i = \|C_{n_i} - C_{m_i}\|_1$.

TABLE 1
Measures of Incorrect Pixels from MS Median Filter and Comparisons with Median Filtering

Shapes	MS	Median filter				
		1	2	3	4	5
Flower R0	26	48	30	27	53	81
Flower R1	18	17	14	13	44	78
Flower R2	6	9	8	20	44	84
Polygon R0	24	51	35	33	39	54
Polygon R1	12	21	17	18	32	39
Polygon R2	6	6	8	12	20	37
Star	111	143	115	117	142	174

The values represent the number of incorrect pixels between ideal perfect images (flower, polygon, and star) and several median filtering of these images corrupted with noise (some of them are illustrated in Figs. 7a, 7b and 7c, and Fig. 1.4). The first column represents the measures obtained with the Meaningful Scale median filter.

Given a point on a maximal segment, the closer its eccentricity is to $\frac{1}{2}$ the more centered it is.

The λ -MST direction at point C_k is the weighted convex combination of the directions of the covering maximal segments:

$$\hat{\theta}(k) = \frac{\sum_{i \in \Gamma(k)} \lambda(e_i(k)) \theta_i}{\sum_{i \in \Gamma(k)} \lambda(e_i(k))},$$

where λ is a mapping from $[0, 1]$ to \mathbb{R}^+ with $\lambda(0) = \lambda(1) = 0$ and $\lambda > 0$ elsewhere. We have chosen here a simple triangle function with peak at 0.5, but other choices are possible.

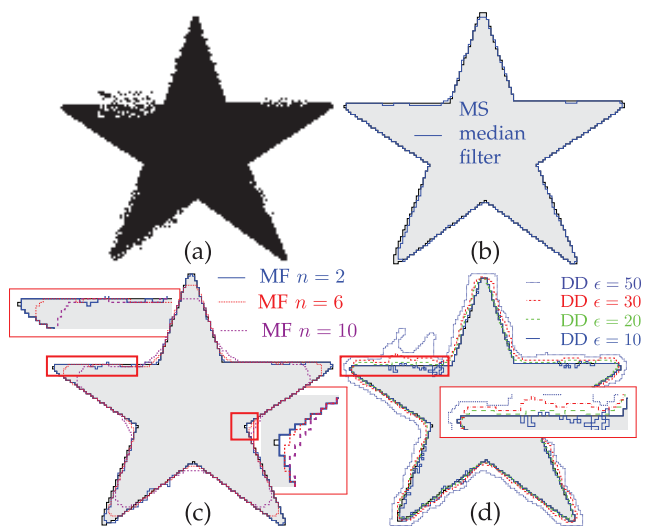


Fig. 14. Result of the adaptive median filter (b) defined with meaningful scales obtained on a noisy star shape (a). The initial star shape is represented in light gray. The images (c) and (d) show, respectively, comparison with a constant size median filter and with the directional denoising approach [34] (denoted as DD) with several values of fidelity parameter ϵ .



Fig. 15. Application of the MS median filter on shapes obtained from nonperfect digitizations (a)-(d). Images (e)-(h) show the resulting shapes obtained without the need to set any parameters.

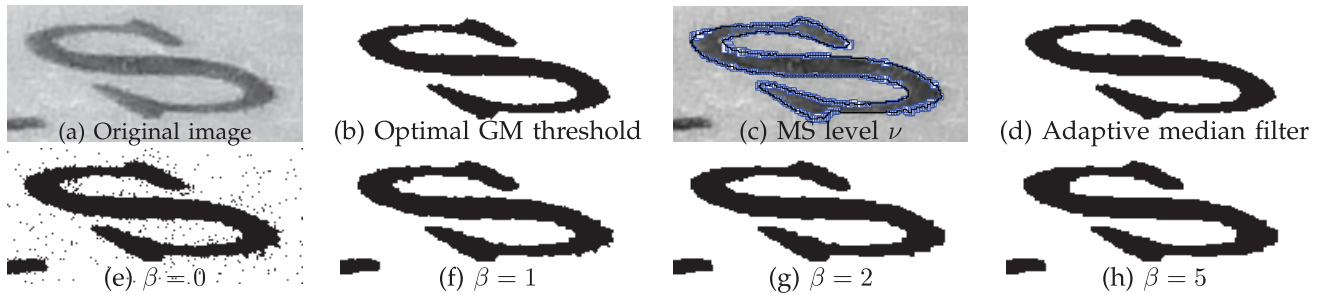


Fig. 16. Comparison of MS median filtering with Markov Random Field segmentation in two classes. Top row: Image (b) gives the optimal Gaussian mixture threshold of (a); image (c) displays the meaningful scale of the digital contour (b), while image (d) displays the induced MS median filtering. Bottom row: Images (e)-(h) display the results of MRF segmentation in two classes, assuming each class follows a normal distribution. The parameter β indicates the balance between the fit to data and the consistency between neighbors. Mean and variance of classes were initialized with the optimal Gaussian mixture threshold. The MRF was optimized with simulated annealing with initial temperature 10, which was stopped after 3,300 iterations.

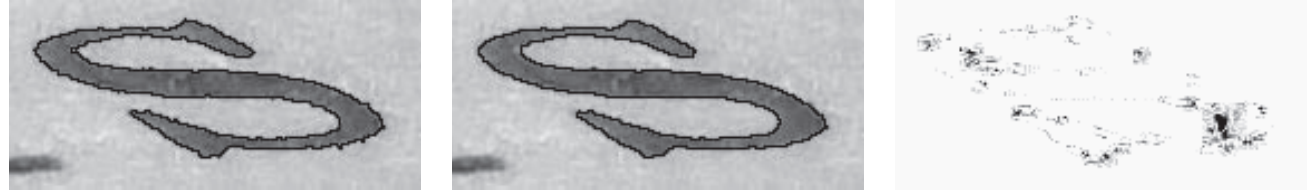


Fig. 17. Local contour restoration with MS median filtering. Left: Original image with isocontour 140 drawn in black (the contour of Fig. 16b). Middle: The same image after adaptive median filtering based on meaningful scale detection (Fig. 16c); isocontour 140 drawn in black. Right: Difference of the two images with contrast enhanced.

To exploit the meaningful scales in the tangent estimation we simply assign to any point C_k the tangent computed from the contour given at the associated meaningful scale (i.e., computed from $\phi_{\nu(C_k)+1}^{0,0}(C)$). The λ -MST estimation on the flower and polygon shapes of Fig. 7 is displayed in Figs. 18a, 18c, 18e, and 18f). Noisy parts are well identified and at the same time relevant features are preserved. The tangent estimation defined through the meaningful scales gives robust estimations on noisy parts and keeps the finest accuracy elsewhere Figs. 18b, 18d, 18g, and 18h). We also compared the estimation obtained from meaningful scales with the λ -MST estimation computed at global scales 4 and 8. The noise disappears too; however, the smoothing effect is well visible near sharp features Figs. 18g and 18h).

5.3 Polygonal Reconstruction

Another potential application of the meaningful scales can be found in numerous polygonal reconstruction methods

for which a scale parameter needs to be set by the user. To demonstrate this application we first consider the algorithm proposed by Bhowmick and Bhattacharya [18], which uses a scale parameter (τ) to adjust the accuracy of the reconstruction process (called ADSS). We applied this algorithm by changing the scale parameter from 1 to 20 with noisy versions of the kangaroo shape illustrated in Fig. 19. Two types of measure were performed on the initial shape. The first one is the Hausdorff distance between the resulting polygon and the digital source contour and the second one is the error of the tangent vectors deducted from the polygon to the ones estimated with the previous λ -MST estimator (see Figs. 19b and 19c)). The same procedure was defined with the polygonalization method called Visual Curvature (VC) [19] (Fig. 19d, 19e, and 19f), which is defined from a given scale.

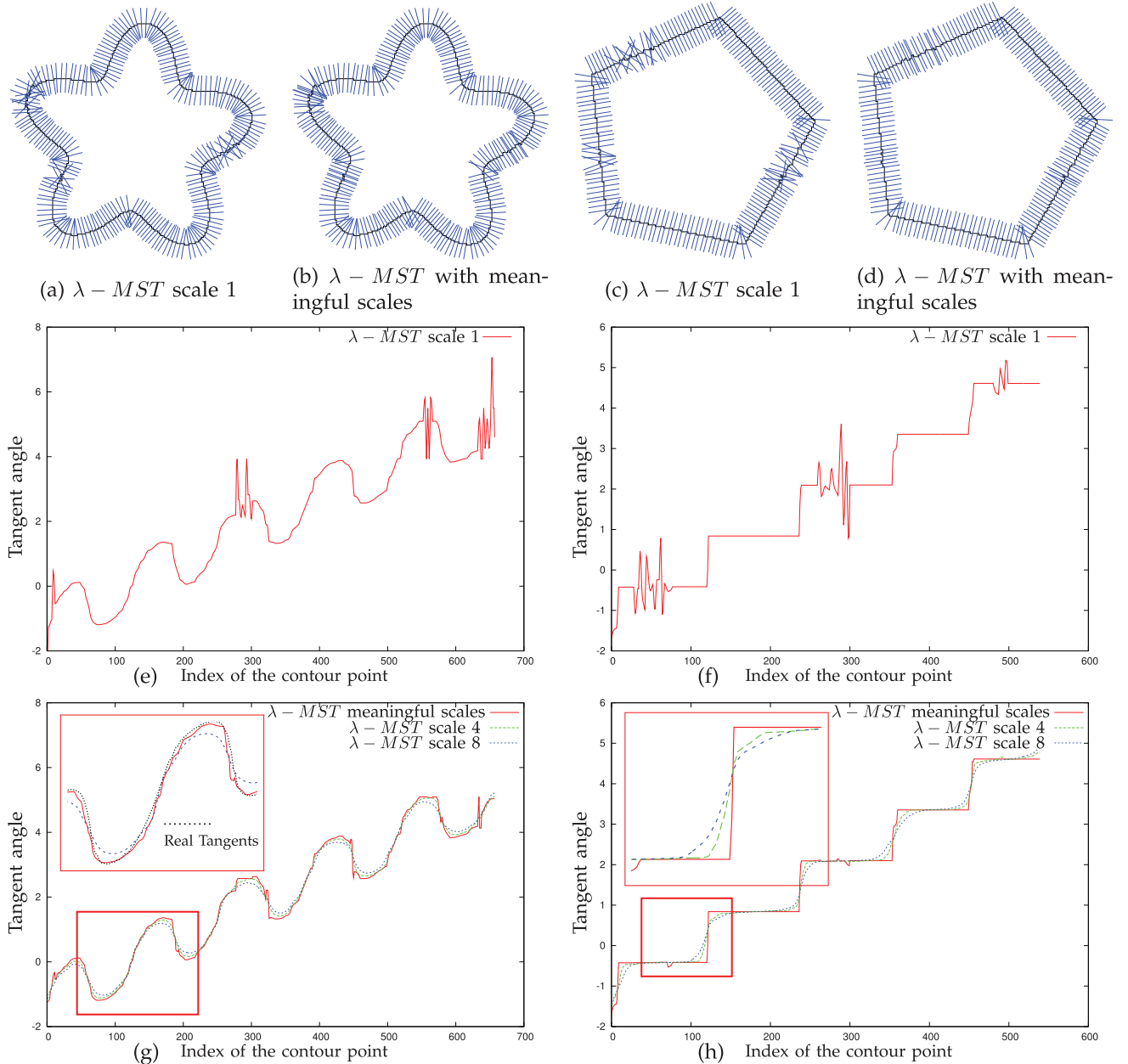


Fig. 18. Normal estimation using the λ -MST estimator combined with meaningful scales. For each shape the estimation obtained at a single scale is given for comparisons (a), (c), and (e)-(h).

As shown in Fig. 19, the use of the mean value of the meaningful scale ν represented by vertical lines in graphics Figs. 19b, 19c, 19e, and 19f gives a Hausdorff error always near the minimal values for each noisy shape. From the point of view of the tangent estimation errors, the use of the parameter 2ν appears to ensure a quasi-minimal error. The choice between ν and 2ν should be defined according to the need of the application and a promising solution to avoid this tradeoff should be to integrate the meaningful scales directly in the polygonalization method.

5.4 Segmentation Evaluation and Improvement

Digital contours can result from a segmentation process such as the watershed algorithms after a region boundary tracking. The automatic evaluation of the amount of noise can be significant to locally evaluate the quality of the

segmentation process. To illustrate this potential use, we applied the meaningful scale detection on the result of the recent approach called the *power watershed* [20] (Fig. 20). The comparisons between the error made by the segmentation (areas highlighted in red in Figs. 20b and 20d) and the noise detection (Fig. 20a and 20c) shows that this detection can be useful to improve shape segmentation approaches.

6 CONCLUSION

The original and simple notion of meaningful scales proposed in this paper offers new possibilities to automatically detect what the local pertinent scales of a discrete contour are. If a meaningful scale interval exists given a maximal scale, it is possible to obtain geometric information as the curvedness/flatness even on noisy contours.

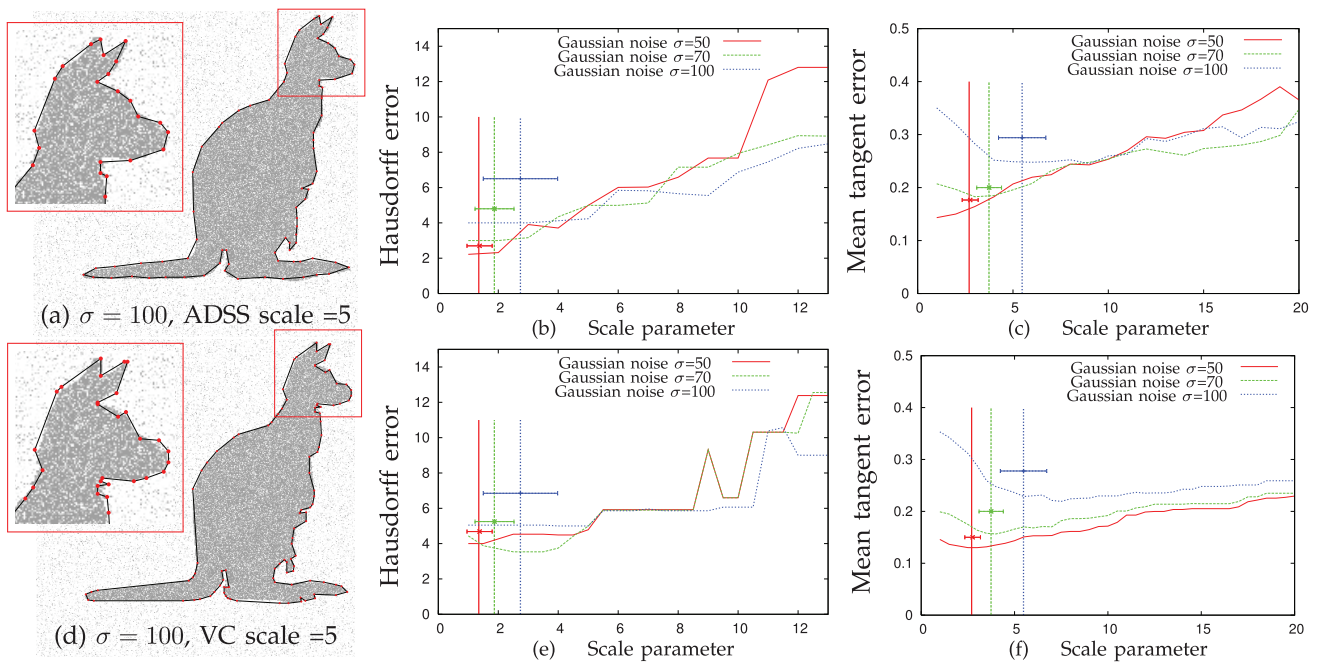


Fig. 19. Polygonalization from meaningful scales by using the Bohwmick and Bhattacharya algorithm [18] (a)-(c) and by using the Visual Curvature-based polygonalization [19] (d)-(f). The experiments were obtained on three digital contours extracted from noisy images (with Gaussian noise $\sigma = 50, 70, 100$; see images (a) and (d)). The measure of Hausdorff distance between the polygonal reconstruction and the source shape is represented in (b) and (e) with the associated meaningful scale level ν represented by vertical lines. The graphics (c) and (f) show the error between the tangent vector from the polygonal shape and the tangents estimated by the λ -MST estimator. The illustrating scales 2ν are drawn by vertical lines in (c) and (f).

Moreover it provides a tool for unsupervised noise detection which allows us to locally detect the amount of noise on fine or coarse resolution shapes. The direct applications of this concept to contour denoising and

geometric estimation already demonstrate the potential of the approach. In future work, we plan to adapt this concept to the blurred segments primitive and to extend the meaningful scales to 3D objects.

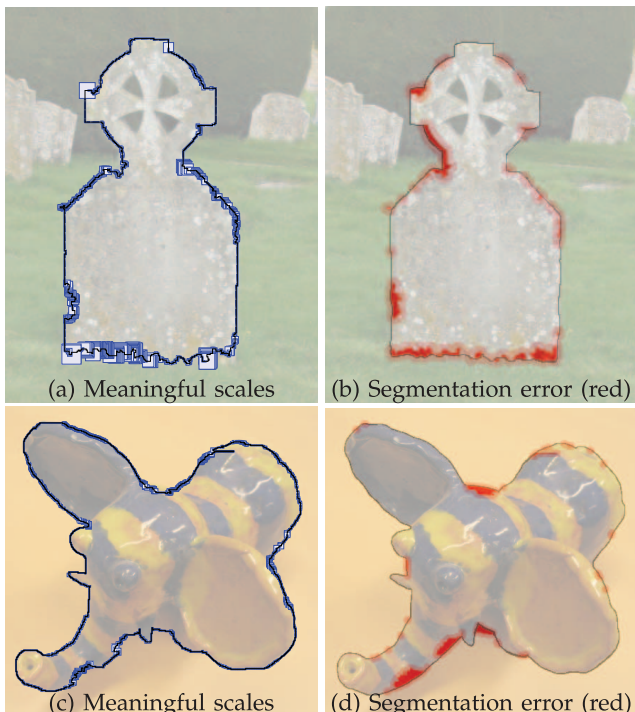


Fig. 20. Application of meaningful scale detection on the result of the power watershed segmentation approach [20] (a) and (c) and comparisons with segmentation error highlighted in red (b) and (d).

ACKNOWLEDGMENTS

The authors would like to thank Partha Bhowmick and Bhargab B. Bhattacharya for providing the source code of the polygonalization technique based on the notion of Approximate Digital Straight line Segments [18]. They also thank Salvatore Tabbone and Thai Van Hoang for performing experiments for comparisons [34] and the anonymous reviewers and the editor for their many constructive and valuable comments, questions, and suggestions that really helped to improve this paper.

REFERENCES

- [1] I. Debled-Rennesson, F. Feschet, and J. Rouyer-Degli, "Optimal Blurred Segments Decomposition of Noisy Shapes in Linear Times," *Computers and Graphics*, vol. 30, pp. 30-36, 2006.
- [2] T. Nguyen and I. Debled-Rennesson, "Curvature Estimation in Noisy Curves," *Proc. 12th Int'l Conf. Computer Analysis of Images and Patterns*, pp. 474-481, 2007.
- [3] B. Kerautret and J.-O. Lachaud, "Curvature Estimation along Noisy Digital Contours by Approximate Global Optimization," *Pattern Recognition*, vol. 42, no. 10, pp. 2265-2278, Oct. 2009.
- [4] R. Malgouyres, F. Brunet, and S. Fourey, "Binomial Convolutions and Derivatives Estimations from Noisy Discretizations," *Proc. 14th Int'l Conf. Discrete Geometry for Computer Imagery*, pp. 370-379, Apr. 2008.
- [5] M. Marij, "On the Detection of Dominant Points on Digital Planar Curves," PhD dissertation, Wayne State Univ., 2003.
- [6] L. Rudin, S. Osher, and E. Fatemi, "Nonlinear Total Variation Based Noise Removal Algorithms," *Physica D*, vol. 60, pp. 259-268, 1992.

- [7] A.P. Witkin, "Scale-Space Filtering," *Proc. Eight Int'l Joint Conf. Artificial Intelligence*, pp. 1019-1022, 1983.
- [8] J.J. Koenderink, "The Structure of Images," *Biological Cybernetics*, vol. 50, pp. 363-370, 1984.
- [9] H. Jeong and C. Kim, "Adaptive Determination of Filter Scales for Edge Detection," *IEEE Trans. Pattern Analysis and Machine Intelligence*, vol. 14, no. 5, pp. 579-585, May 1992.
- [10] D. Mumford and J. Shah, "Optimal Approximations by Piecewise Smooth Functions and Associated Variational Problems," *Comm. Pure Applied Math.*, vol. 42, pp. 577-684, 1989.
- [11] J. Elder and S.W. Zucker, "Local Scale Control for Edge Detection and Blur Estimation," *IEEE Trans. Pattern Analysis and Machine Intelligence*, vol. 20, no. 7, pp. 669-716, July 1998.
- [12] C. Kervrann, "An Adaptive Window Approach for Image Smoothing and Structures Preserving," *Proc. Ninth European Conf. Computer Vision*, pp. 132-144, 2004.
- [13] P. Perona and J. Malik, "Scale-Space and Edge Detection Using Anisotropic Diffusion," *IEEE Trans. Pattern Analysis and Machine Intelligence*, vol. 12, no. 7, pp. 629-639, July 1990.
- [14] D. Barash, "A Fundamental Relationship between Bilateral Filtering, Adaptive Smoothing and the Nonlinear Diffusion Equation," *IEEE Trans. Pattern Analysis and Machine Intelligence*, vol. 24, no. 6, pp. 844-847, June 2002.
- [15] K. Chen, "Adaptive Smoothing via Contextual and Local Discontinuities," *IEEE Trans. Pattern Analysis and Machine Intelligence*, vol. 27, no. 10, pp. 1552-1566, Oct. 2005.
- [16] A. Goshtasby and M. Satter, "An Adaptive Window Mechanism for Image Smoothing," *Computer Vision and Image Understanding*, vol. 111, pp. 155-169, 2008.
- [17] J.-O. Lachaud, A. Vialard, and F. de Vieilleveille, "Fast, Accurate and Convergent Tangent Estimation on Digital Contours," *Image Vision Computing*, vol. 25, no. 10, pp. 1572-1587, Oct. 2007.
- [18] P. Bhowmick and B.B. Bhattacharya, "Fast Polygonal Approximation of Digital Curves Using Relaxed Straightness Properties," *IEEE Trans. Pattern Analysis and Machine Intelligence*, vol. 29, no. 9, pp. 1590-1602, Sept. 2007.
- [19] H. Liu, L.J. Latecki, and W. Liu, "A Unified Curvature Definition for Regular, Polygonal, and Digital Planar Curves," *Int'l J. Computer Vision*, vol. 80, no. 1, pp. 104-124, 2008.
- [20] C. Couprise, L. Grady, L. Najman, and H. Talbot, "Power Watersheds: A Unifying Graph-Based Optimization Framework," *IEEE Trans. Pattern Analysis and Machine Intelligence*, vol. 33, no. 7, pp. 1384-1399, July 2011.
- [21] B. Kerrouetret and J.-O. Lachaud, "MS Online Demonstration," <http://kerrecherche.iutsd.uhp-nancy.fr/meaningfulBoxes>, 2010.
- [22] A. Rosenfeld, "Digital Straight Line Segments," *IEEE Trans. Computers*, vol. 23, no. 12, pp. 1264-1269, Dec. 1974.
- [23] L. Dorst and A. Smeulders, "Discrete Representation of Straight Line," *IEEE Trans. Pattern Analysis and Machine Intelligence*, vol. 6, no. 4, pp. 450-463, July 1984.
- [24] A. Bruckstein, "Self-Similarity Properties of Digitized Straight Lines," *Contemporary Math.*, vol. 119, pp. 1-20, 1991.
- [25] R. Klette and A. Rosenfeld, "Digital Straightness—A Review," *Discrete Applied Math.*, vol. 139, nos. 1-3, pp. 197-230, 2004.
- [26] I.D. Rennesson and J.-P. Reveilles, "A Linear Algorithm for Segmentation of Digital Curves," *Int'l J. Pattern Recognition Artificial Intelligence*, vol. 9, no. 6, pp. 635-662, 1995.
- [27] R. Klette and A. Rosenfeld, "Grids and Digitization," *Digital Geometry: Geometric Methods for Digital Picture Analysis*, chapter 2, Morgan Kaufmann, 2004.
- [28] J.-O. Lachaud, "Espaces Non-Euclidiens et Analyse d'Image: Modèles Déformables Riemanniens et Discrets, Topologie et Géométrie Discrète," *Habilitation à Diriger des Recherches*, Université Bordeaux 1, in French, 2006.
- [29] B. Kerrouetret and J.-O. Lachaud, "Online Annex of Article: Meaningful Scales Detection along Digital Contours for Unsupervised Local Noise Estimation," <http://www.loria.fr/~kerrouet/annexMeaningfulScalesPAMI.pdf>, Oct. 2011.
- [30] B. Kerrouetret and J.-O. Lachaud, "Multi-Scale Analysis of Discrete Contours for Unsupervised Noise Detection," *Proc. 13th Int'l Workshop Combinatorial Image Analysis*, pp. 187-200, 2009.
- [31] F. de Vieilleveille, J.-O. Lachaud, and F. Feschet, "Maximal Digital Straight Segments and Convergence of Discrete Geometric Estimators," *J. Math. Imaging Vision*, vol. 27, no. 2, pp. 471-502, Feb. 2007.
- [32] T. Kanungo, "Document Degradation Models and a Methodology for Degradation Model Validation," PhD dissertation, Univ. of Washington, 1996.
- [33] A.C. Bovik, *Handbook of Image and Video Processing*. Academic Press, 2005.
- [34] T.V. Hoang, E.H. Barney Smith, and S. Tabbone, "Edge Noise Removal in Bilevel Graphical Document Images Using Sparse Representation," *Proc. IEEE 18th Int'l Conf. Image Processing*, 2011.



Bertrand Kerrouetret received the PhD degree in computer science from the Bordeaux I University, France, in 2004. Currently, he is working as a professor assistant in computer science at Nancy University (IUT of Saint Dié des Vosges, France) and works in the LORIA laboratory. His research interests include computer vision problems as 3D shape reconstruction or image analysis and discrete geometry. He also works on discrete geometric estimators adapted to noisy discrete objects and to their applications. He is also interested to the applications of computer vision to archaeological and medical imaging.



Jacques-Olivier Lachaud graduated in computer science from ENSIMAG engineering school, in 1994 and received the PhD degree in computer science from Joseph Fourier University Grenoble, France, in 1998. Currently, he is working as a computer science professor at the University of Savoie, Chambéry, France, and works in the mathematics laboratory (LAMA). His research interests include image segmentation and analysis, more specifically, deformable models, energy-minimizing techniques, digital geometry, topological models, and invariants. He has published more than 60 papers in international journals or conferences on these topics.

▷ For more information on this or any other computing topic, please visit our Digital Library at www.computer.org/publications/dlib.